ACCSCIENCE PUBLISHING

International Journal of Bioprinting

RESEARCH ARTICLE

Chondrocyte spheroid-laden microporous hydrogel-based 3D bioprinting for cartilage regeneration

Ruiquan Liu[1], Litao Jia[2], Jianguo Chen[1],Yi Long[3], Jinshi Zeng[1], Siyu Liu[2], Bo Pan[1], Xia Liu[2]*, and Haiyue Jiang[1]*

[1]Department of Auricular Reconstruction, Plastic Surgery Hospital, Chinese Academy of Medical Sciences and Peking Union Medical College, Beijing 100144, China

[2]Research Center of Plastic Surgery Hospital, Chinese Academy of Medical Sciences and Peking Union Medical College, Beijing 100144, China

[3]Department of Biomedical Engineering, School of Medicine, Tsinghua-Peking Center for Life Sciences, Tsinghua University, Beijing 10084, China

Abstract

Three-dimensional (3D) bioprinting has brought new promising strategies for the regeneration of cartilage with specific shapes. In cartilage bioprinting, chondrocyte-laden hydrogels are the most commonly used bioinks. However, the dispersion of cells and the dense texture of the hydrogel in the conventional bioink may limit cell–cell/cell–extracellular matrix (ECM) interactions, counting against cartilage regeneration and maturation. To address this issue, in this study, we developed a functional bioink for cartilage bioprinting based on chondrocyte spheroids (CSs) and microporous hydrogels, in which CSs as multicellular aggregates can provide extensive cell–cell/cell–ECM interactions to mimic the natural cartilage microenvironment, and microporous hydrogels can provide space and channel for the growth and fusion of the CSs. Firstly, we used a non-adhesive microporous system to produce homogeneous self-assembled CSs in high-throughput and evaluated the influence of different CSs preparation parameters (cell number and culture time) on CSs, which aids in the preparation of bioink suitable for cartilage bioprinting. Then, polyethylene oxide (PEO) was introduced into gelatin methacrylate (GelMA) to prepare microporous hydrogel. Finally, the CS-laden microporous hydrogels were printed, and the constructs were implanted into nude mice. The results showed that the CSs with 500 cells cultured for 1 day exhibited better proliferation and growth ability in microporous hydrogels compared to those with more cells and cultured for longer time. In addition, the results also demonstrated that the CS-laden bioink can be successfully printed into predefined lattice-shape constructs with little cell damage and regenerated cartilage tissue *in vivo* with a structure similar to natural cartilage characterized by typical lacunae structure and abundant cartilage-specific ECM deposition. In summary, our study verified the feasibility and advantages of using CSs as building blocks in cartilage bioprinting, which provides novel strategies for the fabrication and regeneration of patient-specific shaped cartilage.

Keywords: 3D bioprinting; Chondrocyte spheroids; Microporous hydrogels; Cartilage regeneration

***Corresponding authors:**
Haiyue Jiang
(jianghaiyue@psh.pumc.edu.cn)

Xia Liu
(liuxia@psh.pumc.edu.cn)

Citation: Liu R, Jia L, Chen J, *et al*., 2023, Chondrocyte spheroid-laden microporous hydrogel-based 3D bioprinting for cartilage regeneration. *Int J Bioprint*. https://doi.org/10.36922/ijb.0161

Received: May 11, 2023
Accepted: June 14, 2023
Published Online: July 28, 2023

1. Introduction

The repair of cartilage defects, such as the defects in ears and nose, has always been a great challenge faced by plastic surgeons. Currently, the mainstream approach to this challenge is autologous cartilage transplantation, but it has some restrictions such as limited donor tissue, damaged donor site, and high technical requirements[1].

The development of cartilage tissue engineering and three-dimensional (3D) bioprinting technology has brought new possibilities for obtaining large volumes of cartilage tissue with specific complex shapes, that is, using bioinks for 3D bioprinting to regenerate engineered cartilage tissue of desired shape[2-5]. The most commonly used bioinks for cartilage bioprinting are a mixture of expanded chondrocytes and biocompatible hydrogels, with the advantages of easy preparation and uniform cell distribution[6,7]. However, some scholars have pointed out that seed cells in such bioinks are usually dispersed and separated from each other due to the use of cell suspensions and the trapping effect of hydrogels, and this would result in the prevalence of cell–hydrogel interactions but diminished cell–cell and cell–extracellular matrix (ECM) interactions[8-10]. Also, they noted that although natural hydrogels (e.g., collagen, gelatin, etc.) can provide more biological information than synthetic polymers to guide cell function and behavior, this information is not as dynamic and complex as the biological information provided by adjacent cells or ECM and often cannot elicit the greatest repertoire of cell functions. Moreover, it has been reported that during the formation and maturation of natural cartilage, the cell–cell/cell–ECM interactions played an important role in initiating cartilage differentiation and regulating the phenotype of chondrocytes[11,12].

In recent years, some researchers have proposed the use of chondrocyte spheroids (CSs) instead of dispersed chondrocytes as cell supplements to prepare bioinks[13-15]. CSs are multi-cellular aggregates formed by the self-assembly of chondrocytes, which have extensive cell–cell/cell–ECM interactions and can well mimic the microstructural characteristics and extracellular microenvironment of natural cartilage[16,17]. For the effect of using CSs, Huang *et al.*[18] pointed out that the spheroid culture of chondrocytes can promote cell redifferentiation and enhance cell function. Jeon *et al.*[19] observed that injecting CSs into cartilage defect areas resulted in better cartilage regeneration compared to dispersed cells. Wang *et al.*[20] found that the use of CSs facilitated the maintenance of cell phenotype in hydrogels. Notably, although the above-mentioned studies suggested that the use of CSs to replace dispersed chondrocytes may be beneficial, until now, few studies have reported in detail on the application of CS-laden bioink in bioprinting engineered cartilage with specific shapes, especially in its feasibility of bioprinting and ability to regenerate cartilage *in vivo*. Meanwhile, in previous studies, the cell number and culture time used for the preparation of CSs varied greatly[17,19-21], which may have a significant influence on the performance of CSs in cartilage regeneration, so there is a necessity to clarify the effect of these two parameters on CSs before using CS-laden bioinks for cartilage printing.

In addition, the basic elements of bioinks for 3D printing are not only cell supplements but also hydrogels. However, as mentioned above, commonly used hydrogels, such as gelatin methacrylate (GelMA) and hyaluronic acid methacrylate (HAMA), usually have a trapping effect, that is, the dense network of biomaterials inside the hydrogels can limit cell migration, proliferation, and ECM deposition, thus hindering the establishment cell–cell and cell–ECM interactions[22,23]. To address this issue, we propose using polyethylene oxide (PEO), a non-toxic inert pore agent[23,24], to generate a large number of micropores in GelMA, which could provide space for the establishment of cell–cell/cell–ECM interactions.

To summarize, in this study, we developed a novel bioink for cartilage bioprinting using CSs and microporous hydrogels (GelMA+PEO), while investigating the influence of the CSs preparation parameters (cell number and culture time) on CSs and the feasibility and effectiveness of this CS-laden microporous bioink in the bioprinting of engineered cartilage.

2. Materials and methods

2.1. Materials and animals

GelMA and lithium phenyl-2,4,6-trimethyl-benzoyl phosphinate (LAP) were purchased from SunP Biotech (Beijing, China). PEO powder was purchased from Sigma Aldrich (St. Louis, USA). Fetal bovine serum (FBS), penicillin–streptomycin–neomycin (PSN) antibiotic, ultrapure agarose, trypsin-ethylenediaminetetraacetic acid (EDTA), Quant-iT™ PicoGreen® dsDNA assay kit, collagen II monoclonal antibody, and TRIzol™ Reagent were purchased from Thermo Fisher Scientific (MA, USA). High-glucose Dulbecco's modified eagle medium (DMEM) and Dulbecco's phosphate-buffered saline (DPBS) were purchased from BasalMedia Technologies (Shanghai, China). Calcein-AM/Propidium Iodide (PI) Double Staining Kit was purchased from Dojindo Laboratories (Kumamoto, Japan). 4',6- Diamidino-2-phenylindole (DAPI) was purchased from Beyotime Biotechnology (Shanghai, China). Polydimethylsiloxane (PDMS) was purchased from Dow Corning (MI, USA). Gelatin was purchased from Sinopharm (Shanghai, China). Tissue

glycosaminoglycan (GAG) total content dimethylmethylene blue (DMMB) kit was purchased from GENMED Scientifics (Boston, USA). Hydroxyproline (HYP) assay kit was purchased from Nanjing Jiancheng Bioengineering (Nanjing, China). Histostain-Plus Immunohistochemical Kit was purchased from NeoBioscience (Shenzhen, China). LightCycler 480 SYBR Green I Master was purchased from Roche (Basel, Switzerland). Oligo(dT)15 Primer, M-MLV Reverse Transcriptase, and dNTP Mix were purchased from Promega Corporation (Wisconsin, USA).

New Zealand white rabbits (male, 4 months old) were purchased from Beijing Long'an Experimental Animal Breeding Center (Beijing, China). BALB/c nude mice (female, 6 weeks old) were purchased from Beijing Vital River Laboratory Animal Technology Co., Ltd (Beijing, China). Animal experiments were approved by the Animal Care and Experiment Committee of Plastic Surgery Hospital.

2.2. Isolation and expansion of auricular chondrocytes

Chondrocytes were obtained from the auricle of the New Zealand white rabbits. The auricular cartilage was minced into 1–2 mm^3 pieces, after removing the soft tissue and perichondrium. Following this, the pieces were digested with 0.25% trypsin-EDTA for 30 min and 0.2% type II collagenase for 6–8 h under continuous agitation at 37°C. The obtained cells were cultured and expanded in a complete medium (high-glucose DMEM supplemented with 10% FBS and 1% PSN) at 37°C with 95% humidity and 5% CO_2. Chondrocytes in passage 2 were used for further experiments.

2.3. Preparation of non-adhesive microwells, formation, and culture of CSs

Non-adherent microwells were fabricated by a double-molding procedure. At first, disc-shaped master mold with a diameter of 30 mm and a height of 3 mm, consisting of 2750 microwells with 400-μm diameter for each well, was designed using AutoCAD (Autodesk, 2022). Each microwell comprised a 200-μm deep cylindrical section and a 200-μm deep hemispherical bottom. According to the design, polytetrafluoroethylene (PTFE) was processed by computer numerical control (CNC) machine tools (T-600S, Taikan, Shenzhen, China) to obtain microporous master molds. Next, the PDMS was poured into the PTFE molds, cured at 65°C for 2 h after degassing, and demolded from them. Then, the sterilized PDMS micropillar molds were placed in a petri dish, and 2% (w/v) ultrapure agarose dissolved in DPBS was heated and poured onto the PDMS molds. Once the agarose molds had solidified after cooling at room temperature, they were punched into a size (33-mm diameter) to fit 6-well plates and separated from the PDMS. Finally, agarose microwell molds with 2750 microwells were transferred into the wells of the 6-well plate, and a little 2% agarose was added around the mold for immobilization. These microwell molds were rinsed with DPBS and stored in a 37°C incubator until use.

For the formation of CSs, chondrocytes were harvested and resuspended, then 1 mL of the appropriate density of cell suspension was added dropwise into each microwell mold. To prepare CSs with different cell numbers, three cell densities were used: 0.55×10^6, 1.375×10^6, and 2.75×10^6 cells/mL, resulting in approximately 200, 500, and 1000 cells per microwell. After the cells had settled into the microwells due to gravity, 4 mL of complete medium was carefully supplemented into each microwell mold, and these 6-well plates were incubated at 37°C with 95% humidity and 5% CO_2. Half of the medium was refreshed every 2 days. Images of each group (200, 500, and 1000 cells/CSs) were taken with a light microscope (T12-U, Nikon, Tokyo, Japan) at 0, 1, 7, and 14 days of culture for morphological evaluation. These images were processed with ImageJ software (version 1.53c, NI Health, Bethesda, MD, USA), and the diameters and areas of the CSs were measured (n = 100). The process of non-adhesive microwells preparation and CSs formation is illustrated in Figure 1.

2.4. Viability, histology, and biochemical analysis of CSs

After 1, 7, and 14 days of culture in microwells, the CSs were collected for viability, histology, and biochemical analysis. The viability of the CSs was assessed using live/dead staining. Briefly, CSs were rinsed with DPBS and incubated for 20 min with Calcein-AM (2 μM) and PI (4.5 μM). In addition, to facilitate the observation of cells within CSs, DAPI was used to label nuclei according to the manufacturer's instructions. These CSs were imaged with an inverted fluorescence microscope (T12-U, Nikon, Tokyo, Japan).

For histology analysis, CSs were fixed in 4% paraformaldehyde for 1 day, pre-embedded with 0.5% agarose (w/v)-1% gelatin (w/v) mixture[25], dehydrated in graded alcohol, embedded in paraffin, and sectioned. Subsequently, sections were stained with hematoxylin and eosin (H&E) and Alcian blue to evaluate the histological structure and glycosaminoglycan (GAG) deposition in the CSs. All histological images were obtained using a digital slice scanner (EasyScan 1, Motic, Xiamen, China).

At each time point, CSs in three independent agarose molds per group (n = 3, each containing 2750 CSs) were collected separately and subjected to DNA and GAG content measurements. The contents of DNA and GAG were measured using Quant-iT™ PicoGreen® dsDNA assay and DMMB assay, respectively.

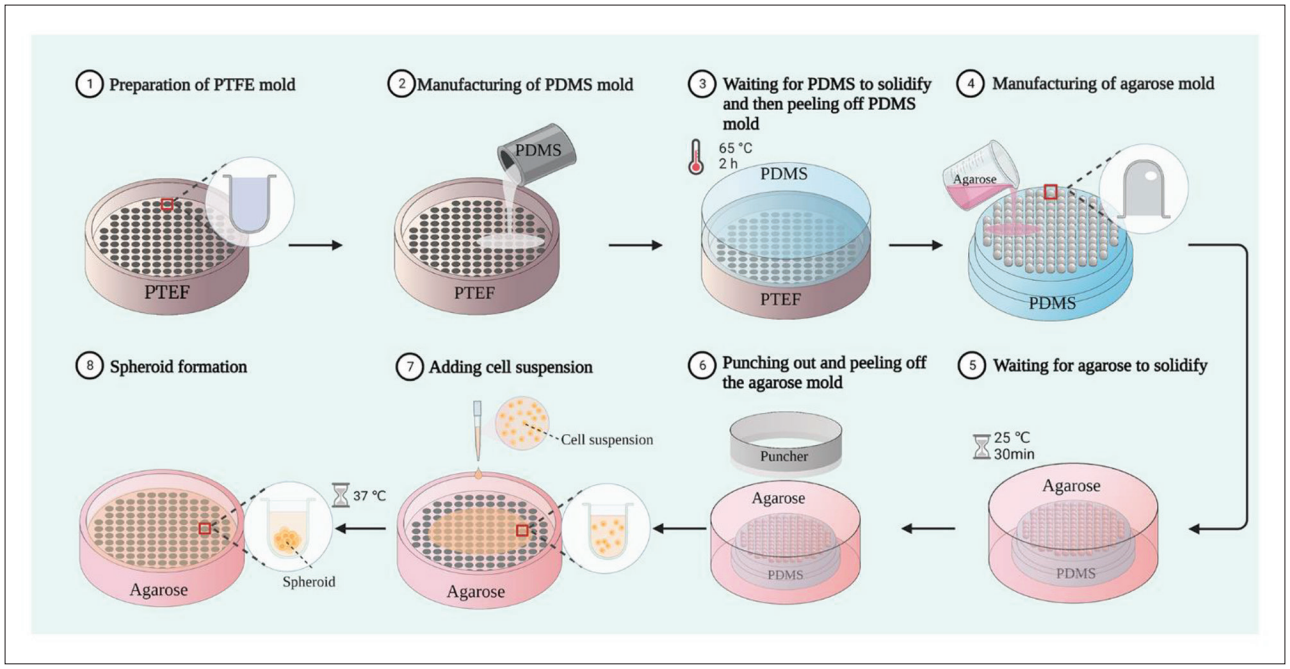

Figure 1. Schematic illustration of the process of non-adhesive microwells preparation and CSs formation.

2.5. Preparation of GelMA with microporous structures

GelMA with microporous structures was prepared using previously established protocols[26]. First, lyophilized GelMA and PEO powder were fully dissolved in the complete medium at 60°C to a final concentration of 10% (w/v) and 1% (w/v), respectively. Then, the dissolved GelMA+PEO solution was sterilized by pasteurization and stored at -20°C in the dark. Before use, LAP was added to a final concentration of 0.25%, and blue light was used to induce photocrosslinking of pre-gel solution (wavelength: 405 nm; light source: LED (Uvata Precision Optoelectronics Co., Ltd.); intensity: 20 mW/cm^2; distance: 10 cm; exposure time: 20 s). In the end, based on the phase separation void-formation strategy, the microporous hydrogels (GelMA+PEO) were immersed in medium to remove the PEO droplets, thus forming microporous structures.

2.6. Characterization, rheological, and mechanical properties of microporous hydrogels

To help evaluate the microporous hydrogels (GelMA+PEO), 10% (w/v) GelMA was chosen for comparison purposes. The micropores in the hydrogels were imaged by confocal microscope (TCS SP8 CARS, Leica, Wetzlar, Germany) after rhodamine B staining, and the micro-morphology of the hydrogels (after lyophilized and coated with gold) was observed by scanning electron microscopy (SEM, Quanta-200, FEI, Oregon, USA). ImageJ software was used to measure the pore size and porosity of hydrogels.

The swelling test was carried out by immersing the cured hydrogel samples in DPBS for 24 h at 37°C and recording the change in weight of the samples. The swelling ratio is calculated using the following formula:

$$\text{Swelling ratio} = W_{swelling}/W_0 \times 100\% \quad \text{(I)}$$

where $W_{swelling}$ is the weight of the hydrogel samples after swelling in DPBS, and W_0 is the initial weight of the hydrogel samples.

Rheological analysis was performed to evaluate the printability of hydrogels, including shear-thinning behavior and temperature-sensitive property. A rotational rheometer (MCR92, Anton Paar, Graz, Austria) containing parallel plate with a 50-mm diameter and a 1-mm gap setting was used for all measurements. The shear-thinning behavior was assessed by measuring the viscosity change of hydrogels when the shear rate increased from 0.1 to 60 1/s continuously at 25°C. The temperature-sensitive property was evaluated by recording the variation of the storage modulus (G') and loss modulus(G") with increasing temperature in the range of 0–30°C.

The mechanical property was determined by measuring Young's modulus through a biomechanical analyzer (Instron-5967, Canton, MA, USA). Hydrogels of each group were processed to form cylindrical-shaped constructs (10-mm diameter and 2.5-mm thickness) by photocuring in PDMS molds with corresponding cylindrical wells. Once the sample was placed, a constant

Table 1. Grouping based on the cell number forming CS and culture time in microwell mold

Group	Number of cells forming CS (cells)	Culture time in microwell molds (days)
500 D1	500	1
500 D7	500	7
500 D14	500	14
1000 D1	1000	1
1000 D7	1000	7
1000 D14	1000	14

Abbreviation: CS, chondrocyte spheroid.

compressive strain rate of 0.5 mm/min was applied until 80% of the maximal deformation was achieved, and Young's modulus was calculated from the slope of the stress–strain curve at 20%–30% strain.

2.7. Evaluation of different CSs after encapsulation into microporous hydrogels

According to the number of cells forming CSs and the culture time of CSs in the microwells, the CSs were divided into six groups for subsequent experiments (Table 1). Briefly, a well of each group of CSs was harvested, and 2 mL microporous hydrogels were used to resuspend. Then, 200 μL CS-laden hydrogels were cast into cylindrical-shaped constructs (10-mm diameter and 2.5-mm thickness), that is, each structure contains about 275 CSs. These constructs were cultured in a complete medium at 37°C with 95% humidity and 5% CO_2. At 0, 7, and 14 days post-encapsulation, CS-laden constructs were stained with Calcein-AM/PI, and the areas of CSs were measured with ImageJ software (n = 10). In addition, constructs were collected at 0 and 14 days post-encapsulation (n = 3), and DNA content was measured using Quant-iT™ PicoGreen® dsDNA assay.

2.8. Bioprinting of lattice-shaped CS/cell-laden constructs

CS-laden and cell-laden hydrogels were prepared and printed into lattice-like constructs. First, microporous hydrogels were prepared as described above, containing 10% GelMA, 1% PEO, and 0.25% LAP. Then, auricular chondrocytes were collected and prepared as CSs (500 D1) through microwell molds. Subsequently, CSs or cells were mixed with microporous hydrogels respectively to make two bioinks with a concentration of 1.25×10^7 cells/mL. Finally, the lattice-shaped constructs were printed by a 3D-Bioplotter (Envision TEC, Germany) and solidified under blue light irradiation. The printing parameters are summarized in **Table S1** (Supplementary File). All printed constructs were cultured in the complete medium until use.

2.9. Evaluation of constructs *in vitro*

After printing, the diameter of the filament and pore of printed constructs were first measured using ImageJ software to compare the printing accuracy of the two groups of bioinks. Next, the micro-morphology of cells or CSs in the constructs was observed using the SEM. Then, after 3 days of *in vitro* culture, the mechanical properties of the two groups of constructs were calculated as described above. Finally, live/dead staining was used to evaluate cell viability. Since the viability of the cells inside the CSs was difficult to assess, we used a two-photon microscope (AXMP, Nikon, Tokyo, Japan) to compare the viability of CSs before and after printing. Confocal microscopy was used to visually evaluate changes in the encapsulated CSs and cells during 7 days of *in vitro* culture.

2.10. Cartilage regeneration *in vivo*

The printed CS-laden and cell-laden constructs were cultured in a complete medium for 3 days to remove the PEO droplets and then implanted subcutaneously in the back of nude mice to evaluate cartilage regeneration *in vivo*. At 4 and 12 weeks post-implantation, constructs were surgically taken out for subsequent analysis.

2.11. Histological and immunohistochemical analysis

Histological and immunohistochemical analyses were performed as previously described[26]. Constructs were fixed in 4% paraformaldehyde and embedded in paraffin. H&E and Alcian blue were performed according to standard protocols. Three visual fields of Alcian blue were randomly selected, and ImageJ software was used to measure the areas of the scattered CSs and the residual hydrogel areas of constructs. Immunohistochemical staining was performed for type II collagen. Mouse monoclonal antibody against collagen II (MS-306-P1, 1:200) was used, followed by a horseradish peroxidase-conjugated anti-mouse antibody. Diaminobenzidine tetrahydrochloride (DAB, Dako) served as a chromogenic agent. The average optical density (AOD) of type II collagen in each group was calculated using ImageJ software.

2.12. Biochemical and gene expression analysis

Three specimens (n = 3) from each group were collected and subjected to the following analysis. For biochemical analysis, in addition to measuring the DNA and GAG content of the construct according to the above method, the content of HYP, as a unique amino acid in collagen, was determined by the HYP assay kit.

The expression of cartilage-related and proliferation-related genes such as type II collagen alpha 1 (*COL2A1*), aggrecan (*ACAN*), SRY-box transcription factor 9 (*SOX9*), elastin (*ELN*), and proliferating cell nuclear antigen (*PCNA*)

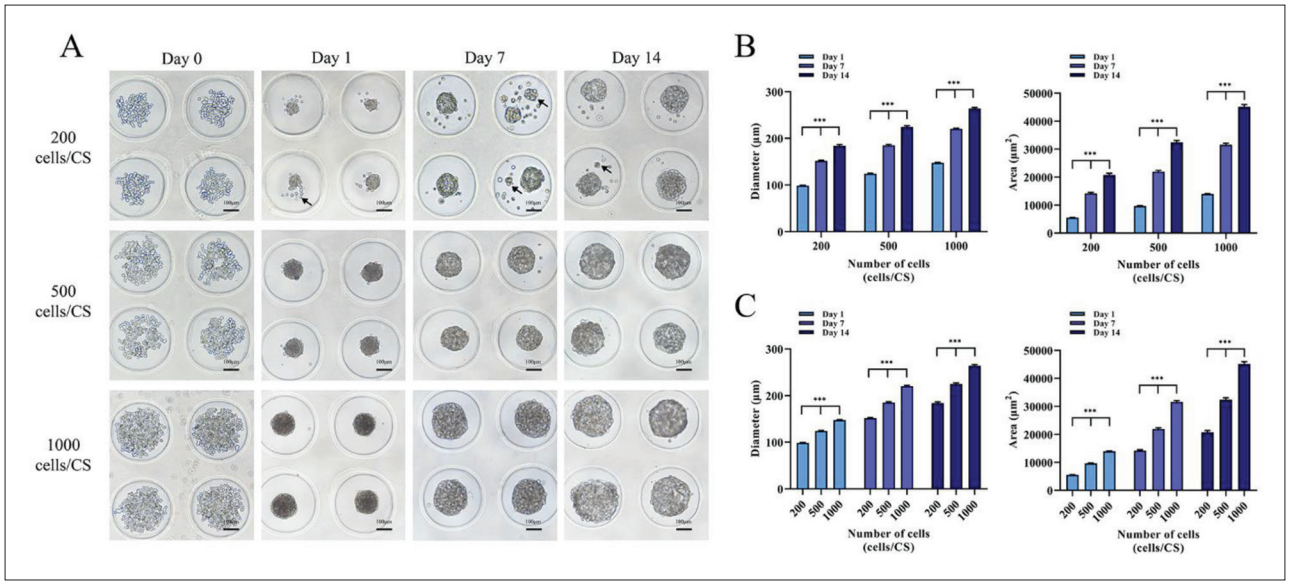

Figure 2. Morphological analysis of CSs. (A) Bright-field images of CSs with different cell numbers cultured in microwells at 0, 1, 7, and 14 days. (B) Comparison of CSs diameter and area at different culture time points. (C) Comparison of diameter and area of CSs with different cell numbers. $^{*}p < 0.05$; $^{**}p < 0.01$; $^{***}p < 0.001$.

was analyzed by quantitative real-time polymerase chain reaction (qRT-PCR). The total RNA of each construct was extracted by TRIzol. Subsequently, the RNA was reverse-transcribed into cDNA, and qRT-PCR detection was performed using the LightCycler® 96 Real-Time PCR system (Roche, Basel, Switzerland) with SYBR Green. The relative expression level of each gene was normalized by the GAPDH expression level and analyzed by the $2^{-\Delta\Delta CT}$ method. The primer sequences used are listed in **Table S2** (Supplementary File).

2.13. Statistical analysis

All experiments were conducted with at least three replicates per group. The continuous variables are presented as the mean ± standard error of mean (S.E.M). Statistical analysis was carried out through GraphPad Prism software (version 9.3.1, GraphPad Software, San Diego, California USA), and the Student's *t*-test or analysis of variance (ANOVA) was selected to test the significance according to the characteristics of the data. A $p < 0.05$ was considered statistically significant.

3. Results and discussion

3.1. Preparation of CSs with different cell numbers and culture times

To examine the influence of cell number and culture time on CSs, the non-adherent microwells method was used in our study because it allows for high-throughput preparation of uniform CSs with controlled cell number and culture time. As shown in Figure 2A–C, CSs with different cell numbers (200, 500, and 1000 cells/CS) and culture times (1, 7, and 14 days) can be prepared in our non-adherent microwell molds, and an increase in both cell numbers and culture times would lead to an enlargement of the CS size (diameter and area). However, it was worth noting that there were more scattered cells and debris around the CSs in the 200 cells/CS group (as indicated with black arrows in Figure 2A) compared with 500 and 1000 cells/CS groups during culture, which may be due to the cell dispersion and insufficient contact among cells in 200 cells/CS group.

3.2. Evaluation of the CSs in each group

Figure 3A presents the results of viability and histological analysis of CSs with different cell numbers and culture times. Live/dead and DAPI staining showed high cell viability and homogeneous cell distribution in all groups of CSs, suggesting no obstruction to nutrient supply in them. H&E and Alcian blue staining showed the longer the culture time, the more GAG deposition in the CSs, but the extent of GAG deposition of CSs with different cell numbers had no obvious difference at each time point. Consistent with the above histological staining results, the biochemical quantification results indicated that the GAG content of each CS increased significantly with culture time (Figure 3B), while after normalization by the DNA content, the GAG/DNA ratio in the 500 and 1000 cells/CS groups had no significant difference (Figure 3D). However, it should be noted that the biochemical analysis also showed that the DNA content of each CS decreased significantly during the first 7 days of culture (Figure 3C), probably due to the difficulty of chondrocyte proliferation in the non-adherent microwells

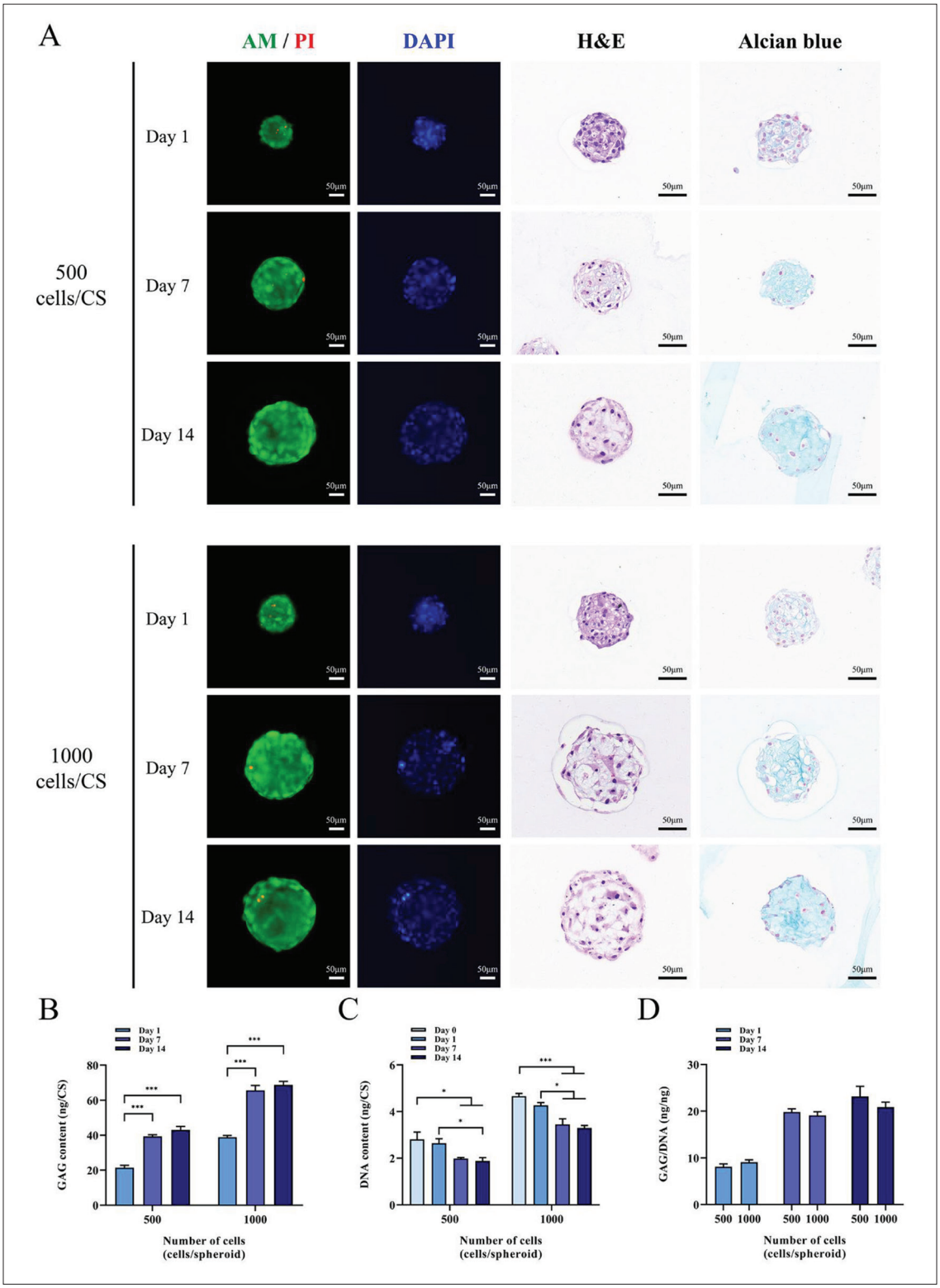

Figure 3. Viability, histological, and biochemical analysis of CSs. (A) Live/dead, DAPI, H&E, and Alcian blue staining of 500 and 1000 cells/CSs at 1, 7, and 14 days of culture in microwells. Biochemical quantitative analysis of (B) GAG content, (C) DNA content, and (D) GAG/DNA of 500 and 1000 cells/CSs during microwells culture. *$p < 0.05$; **$p < 0.01$; ***$p < 0.001$.

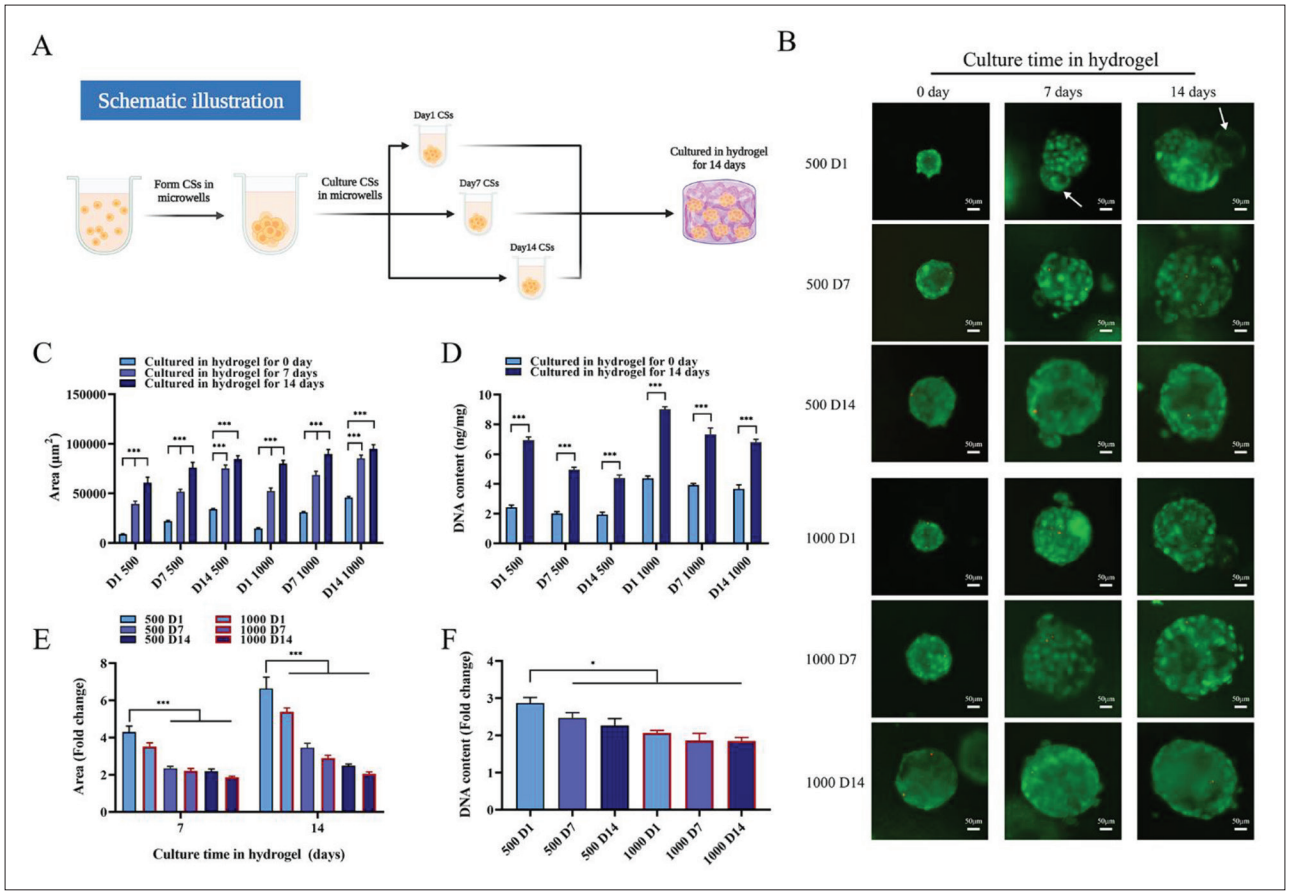

Figure 4. Characterization of microporous hydrogels. (A) Schematic diagrams, optical images, rhodamine B staining, and SEM images of GelMA+PEO (microporous hydrogel) and GelMA. (B) The pore size analysis. (C) The porosity analysis. (D) Swelling ratio. (E) Viscosity–shear rate curve. (F) Modulus–temperature curve. (G) Stress–strain curve. (H) Stress–strain curve (0%–30% strain). (I) Young's modulus. $^{*}p < 0.05$; $^{**}p < 0.01$; $^{***}p < 0.001$.

and the continued death of a small number of cells within CS. The above results suggested that the enlargement of the CSs in non-adherent microwells with culture was due to the continuous secretion of ECM by chondrocytes rather than cell proliferation and that the cell number of CSs had no obvious influence on the GAG secretion function of the chondrocytes if the cells survived well.

3.3. Characterization of microporous hydrogels

As mentioned above, the dense texture of conventional hydrogels is an important factor hindering the establishment of cell–cell/cell–ECM interactions[22,24]. To address this dilemma, in this study, PEO, a non-toxic inert polymer, was introduced into GelMA to prepare the microporous hydrogel based on the phase separation void-formation strategy. Due to the immiscibility of the PEO and the GelMA solutions, the PEO droplets can be leached off after the GelMA crosslinking and consequently form numerous micropores in the cured hydrogels. Rhodamine B staining showed that the introduction of PEO can generate a large number of micropores (dark areas indicated by white arrows in Figure 4A) in GelMA (red fluorescence, emitted by the hydrogel conjugated with rhodamine B). The results of SEM further confirmed that numerous micropores were formed in the GelMA+PEO group, and it is noteworthy that many channels were formed on the walls of these micropores that could connect to the adjacent micropores (as indicated by yellow arrows in Figure 4A). The pore size and porosity analysis revealed that the GelMA+PEO group (72.61 ± 5.30 μm and 63.62% ± 2.25%) had significantly larger pore size and higher porosity than the GelMA group (3.50 ± 0.54 μm and 45.80% ± 1.172%; Figure 4B and C).

Since appropriate swelling, rheological, and mechanical properties are critical for extrusion 3D printing, these properties of microporous hydrogel (GelMA+PEO) were evaluated. For swelling ratio, the results showed that the swelling ratio was 108.1% ± 0.56% for GelMA and 111.6% ± 2.46% for GelMA+PEO, while there was no statistical difference between the two groups (Figure 4D). For the rheological properties, it can be seen from Figure 4E

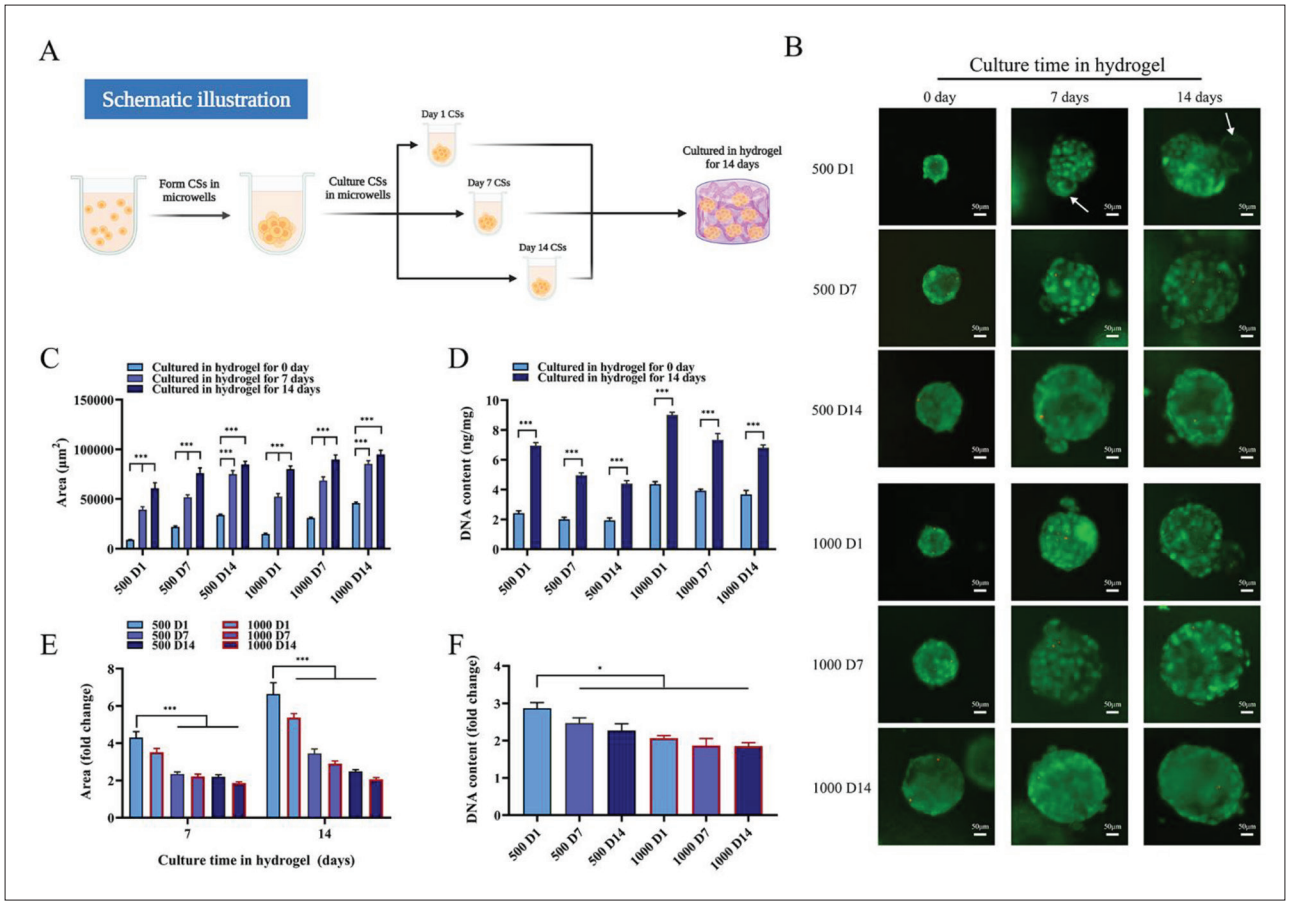

Figure 5. The growth performance of different CSs in microporous hydrogels. (A) Schematic illustration of different CSs cultured in microporous hydrogels. (B) Live/dead staining of each group of CSs after 1, 7, and 14 days of culture in microporous hydrogels. Scale bar: 50 μm. (C) The area of each group of CSs after 1, 7, and 14 days of culture in microporous hydrogels. (D) DNA content of each group of CSs after 1 and 14 days of culture in microporous hydrogels. (E) The fold change of area in each group relative to CSs cultured in hydrogel for 0 day. (F) The fold change of DNA content in each group relative to CSs cultured in hydrogel for 0 day. $^{*}p < 0.05$; $^{**}p < 0.01$; $^{***}p < 0.001$.

that GelMA+PEO has a similar decreasing viscosity with increasing shear rate as GelMA, indicating that it has a good shear-thinning property. Also, as shown in Figure 4F, GelMA+PEO exhibited favorable temperature-sensitive property, which is gel-like (G' > G") when the temperature is lower than the gelling point, and liquid-like (G' < G") when the temperature is higher than the gelling point. Finally, for the mechanical analysis, there was no significant reduction in Young's modulus found in the GelMA+PEO compared with GelMA (Figure 4G–I). These results suggested that the introduction of PEO would not impact the printability and mechanical properties of GelMA and that GelMA+PEO microporous hydrogels can be used for 3D bioprinting of cartilage.

3.4. Evaluation of different CSs after encapsulation into microporous hydrogels

To further clarify the influence of cell number and culture time on CSs, CSs with different cell numbers and culture times (Table 1) were encapsulated in microporous hydrogels and cultured for 14 days (Figure 5A). As shown in Figure 5B, the CSs in all groups survived well for 14 days with few dead cells, and cells in the CSs could sprout into the surrounding micropores (as indicated by white arrows). The morphological and biochemical evaluation showed that the size (area) and DNA content of the CSs in all groups increased with culture in the microporous hydrogels (Figure 5C and D), which was different from the CSs cultured in non-adherent microwells, suggesting the chondrocytes within CSs proliferated in the microporous hydrogel. Notably, the CSs with lower cell numbers and shorter culture times had higher area and DNA content increase folds after encapsulation into the microporous hydrogel, among which the 500 D1 group had the highest increase fold, with a 6.64-fold increase in area and a 2.87-fold increase in DNA content at 14 days (Figure 5E and F). Possible explanations for these results are as follows: (1) The proportion of cells located in the outer layer of the

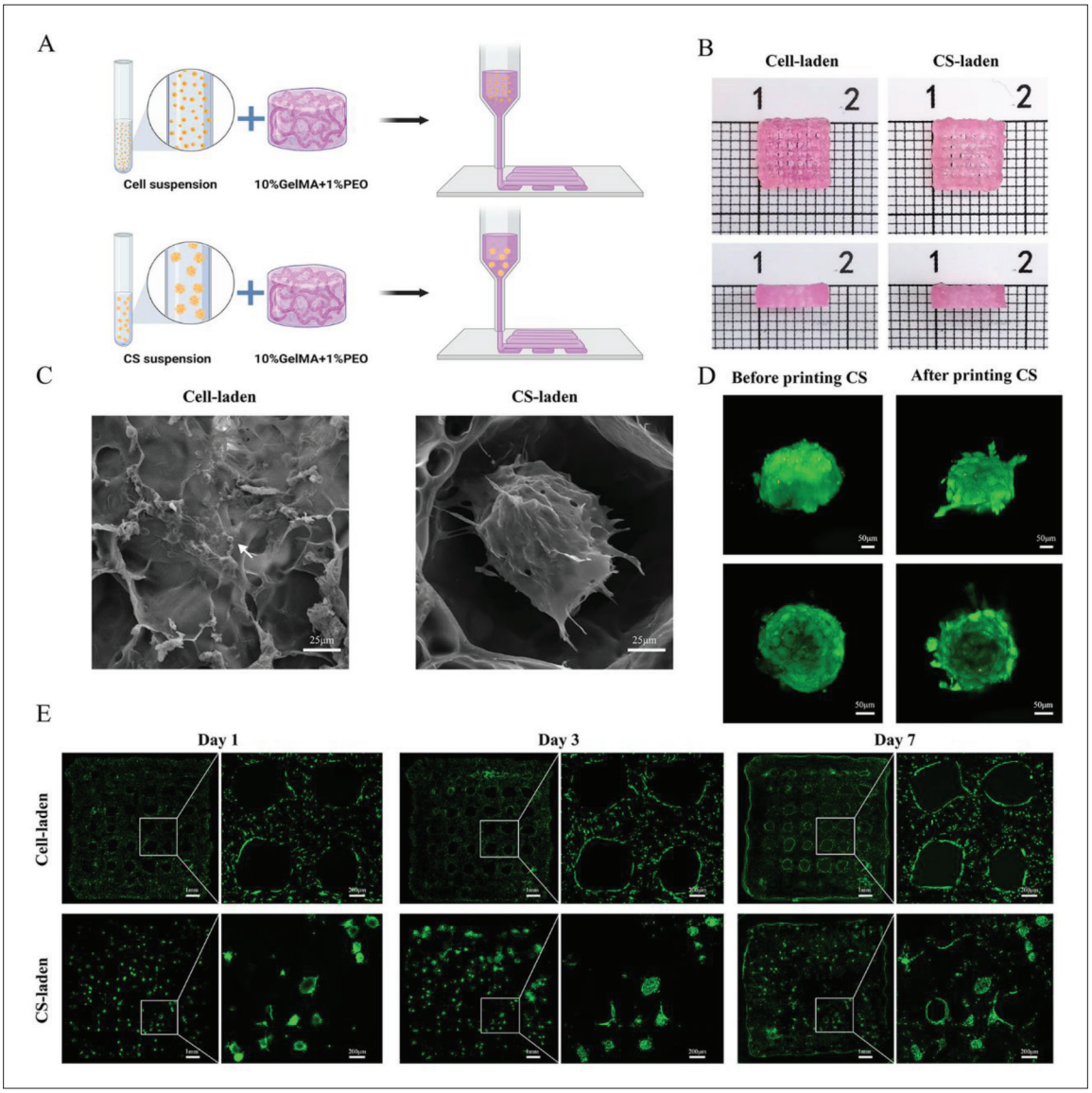

Figure 6. *In vitro* evaluation of printed constructs. (A) Schematic illustration of printing with CS-laden and cell-laden hydrogels. (B) Gross view of printed constructs. (C) SEM images of adherent cells and CSs in the hydrogels after 1 day of printing. Scale bar: 25 μm. (D) Two-photon microscope images of live/dead staining of CSs before and after printing. Scale bar: 50 μm. (E) Live/dead staining of printed constructs cultured *in vitro* for 1, 3, and 7 days. Scale bar: 1 mm (global image) and 200 μm (local magnification image). $^{*}p < 0.05$; $^{**}p < 0.01$; $^{***}p < 0.001$.

spheroids that were more likely to proliferate would decrease as the cell number and size of the spheroids increase[27]. (2) With the culture of spheroids in non-adherent microwells, the progressive deposition of ECM in the spheroids may hinder cell migration and proliferation of spheroids in hydrogels. (3) Many molecules, especially oxygen, have a diffusion limit of 150–200 μm within the spheroids[28,29], so the spheroid enlargement caused by the increase of cell number or culture time would affect the exchange of nutrients within spheroids and cell proliferation[30,31]. Based on the above, we suggested that CSs with low cell numbers and short culture times ought to be used when preparing CS-laden bioinks for cartilage bioprinting. In this study, 500 D1 CSs were selected for subsequent cartilage bioprinting.

3.5. *In vitro* evaluation of printed constructs

The feasibility of bioprinting cartilage with CS-laden microporous bioink was explored by printing lattice-shaped constructs, and cell-laden bioink was used as a control (Figure 6A). The results showed that, like the cell-laden bioink, the CS-laden bioink could be smoothly extruded and printed into the lattice-shaped structure (Figure 6B). Also, there were no significant differences between the

filament and pore diameters of the two groups of printed constructs, which were both close to the parameters of the designed constructs (**Figure S1** in Supplementary File), indicating that the loading of CSs would not affect the bioprinting accuracy. As shown in Figure 6C, SEM revealed that the printed CSs remained intact while the cells in the cell-laden bioink were separated from each other. Mechanical properties testing showed no significant differences in Young's modulus of the two groups of printed constructs (**Figure S2** in Supplementary File), suggesting that the encapsulated CSs or cells had a similar effect on the overall mechanical properties of the constructs. Live/dead staining showed high cell viability in both pre- and post-printed CSs (Figure 6D), and the number of green cells in the CS-laden constructs had increased over time during *in vitro* culture as in the cell-laden constructs (Figure 6E), which demonstrated that bioprinting with CS-laden bioink would not damage the viability and proliferation capacity of chondrocytes in CSs. Although many studies have shown that cell-laden bioinks can be used to construct engineered cartilage by 3D bioprinting[7,26,32], there are still some concerns regarding the use of CSs for bioprinting, such as nozzle clogging and damage to the CSs during the printing process[15,33]. In this study, the successful printing of CSs was attributed to the uniform CSs with diameters smaller than the inner diameter of the nozzle produced by the non-adherent microwell molds and the shear-thinning behavior of the microporous hydrogels.

3.6. *In vivo* cartilage regeneration of printed constructs

Knowing that the *in vivo* cartilage regeneration is the most important criterion to evaluate the performance of a bioink in constructing engineered cartilage, the printed CS-laden and cell-laden constructs were implanted into the nude mice. Figure 7A presents the gross view and histological and immunohistochemical staining of the constructs at 4 and 12 weeks after implantation. After 4 weeks *in vivo*, the constructs in both groups showed a white translucent appearance and maintained their original shape. Histological staining demonstrated that cartilage-like tissues with cartilage lacunae and GAG deposition were regenerated in the constructs of both groups. Notably, there were abundant typical cartilage lacunae in the CS-laden constructs, which were rare in the cell-laden constructs, indicating that the regenerated cartilage in the CS-laden group resembled the natural cartilage in terms of histological structure. Immunohistochemical results showed that the staining of type II collagen was deeper in the CS-laden group than in the cell-laden group (**Figure S3** in Supplementary File), suggesting that chondrocytes in the CS-laden group had a better ability to secrete type II collagen. By 12 weeks, the regenerated cartilage tissues in the CS-laden group showed a milky-white cartilage appearance (as indicated by the white arrows in Figure 7A), and histology results demonstrated that these regenerated cartilage tissues had huge resemblance to the natural cartilage, with good chondrocyte morphology, typical cartilage lacunae, and abundant cartilage-specific ECM. In contrast, the regenerated tissues in the cell-laden group were still quite different from the natural cartilage, especially in terms of cell morphology and maturity of cartilage lacunae, even though the uniform distribution of chondrocyte populations with pericellular ECM deposition could be observed. Meanwhile, the histological results also revealed that the CSs would enlarge over time and fuse with adjacent CSs (**Figures S4** and **S5** in Supplementary File) during *in vivo* culture, which further confirmed the feasibility of CS-laden microporous bioink in the construction of engineered cartilage. However, it should be noted that when comparing the residual hydrogel area within the two groups of constructs, the results showed that the proportion of residual hydrogel was lower in the cell-laden group than in the CS-laden group (**Figure S6** in Supplementary File), possibly implying that there was a higher rate of cell proliferation and hydrogel degradation in the cell-laden group after *in vivo* culture.

Biochemical analyses showed that weight-normalized GAG content, HYP content, and DNA content of the constructs increased with culture in both groups (Figure 7C–E), which is consistent with the histological results that demonstrated the regeneration and maturation of cartilage in both groups. Notably, although the DNA content per unit weight of constructs was higher in the cell-laden group, there was no significant difference between the two groups in the GAG content and HYP content per unit weight of constructs. Moreover, after normalization of GAG content and HYP content by DNA content, the results showed that both GAG/DNA and HYP/DNA ratios were significantly higher in the CS-laden group than in the cell-laden group (Figure 7F and G). These results indicated that chondrocytes in the CS-laden group had a stronger ability to secrete ECM.

To clarify the status of chondrocytes in the constructs *in vivo*, the expressions of cartilage-specific genes (*COL2A1*, *ACAN*, *SOX9*, and *ELN*) and proliferation-related gene (*PCNA*) were detected by qRT-PCR assays (Figure 8A–E). Firstly, the comparison of the expression levels of the above-mentioned genes showed that there was no significant difference in the expression levels of the cartilage-specific genes between the two groups at 4 weeks, but by 12 weeks, the expression levels of these genes were higher in the CS-laden group than in the cell-laden group (Figure 8E). In contrast, the expression level of *PCNA* in the CS-laden constructs was significantly lower than that

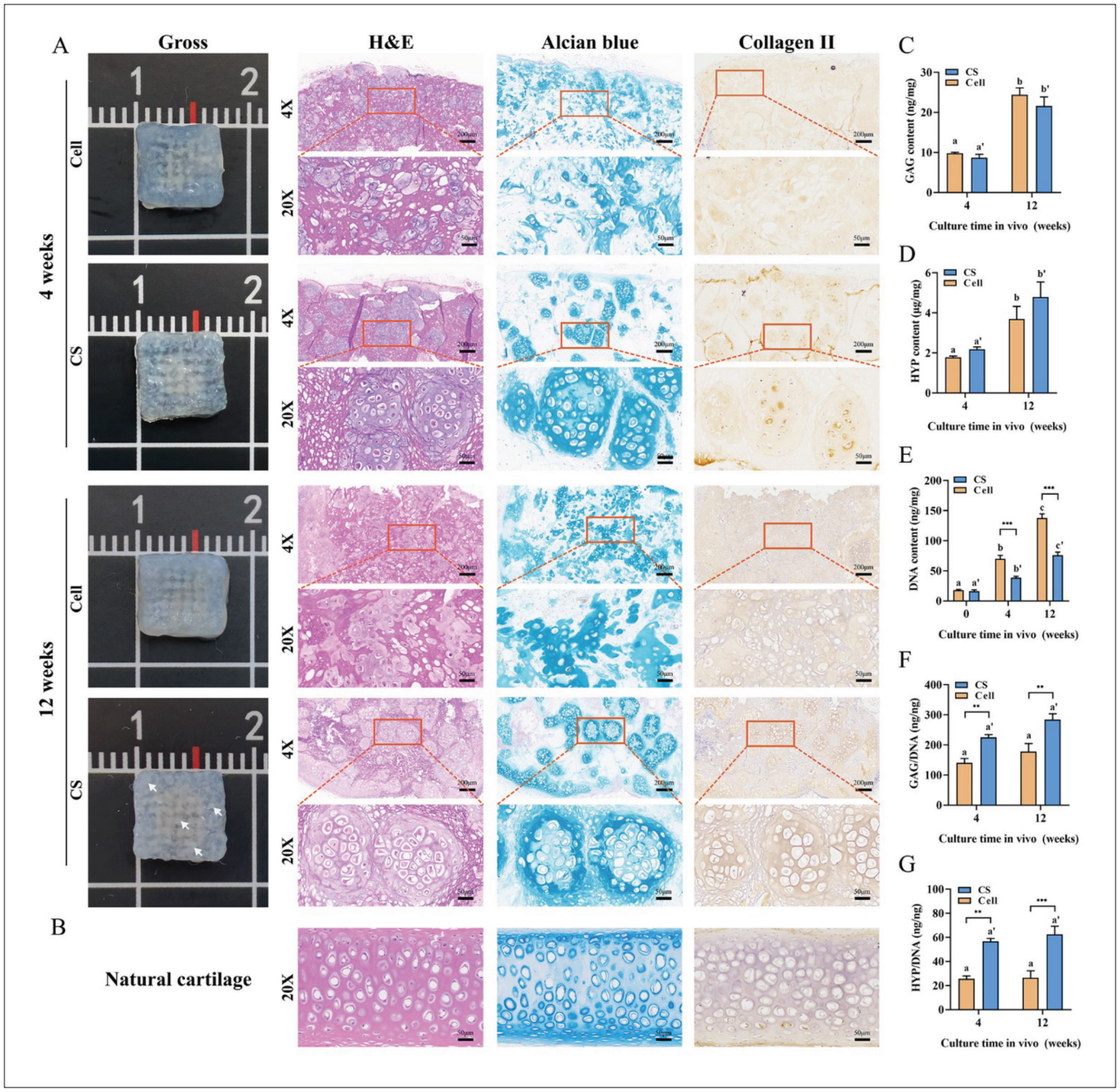

Figure 7. *In vivo* cartilage regeneration of printed constructs. (A) Gross view, H&E staining, Alcian blue staining, and type II collagen immunohistochemical staining of two groups of constructs after 4 and 12 weeks of culture *in vivo*. Scale bar: 200 μm (4X) and 50 μm (20X). (B) H&E staining, Alcian blue staining, and type II collagen immunohistochemical staining of natural cartilage. Scale bar: 50 μm. (C) GAG content of two groups of constructs after 4 and 12 weeks of culture *in vivo*. (D) HYP content of two groups of constructs after 4 and 12 weeks of culture *in vivo*. (E) DNA content of two groups of constructs after 0, 4, and 12 weeks of culture *in vivo*. (F) GAG/DNA of two groups of constructs after 4 and 12 weeks of culture *in vivo*. (G) HYP/DNA of two groups of constructs after 4 and 12 weeks of culture *in vivo*. Statistical analysis of the same group at different culture time is indicated by letters, and indication with different letters represents $p < 0.05$. Statistical analysis between different groups is indicated by asterisks: $^{*}p < 0.05$; $^{**}p < 0.01$; $^{***}p < 0.001$.

in the cell-laden constructs after 4 weeks of *in vivo* culture (Figure 8E). These results are consistent with the findings of biochemical quantification described above. However, different from our results, Wang *et al.* found that the CS-laden GelMA/HAMA construct had better cell proliferation than the cell-laden constructs[20]. This difference may be attributed to the use of PEO-based microporous hydrogels in the current study. Our previous study verified that PEO-assisted microporous hydrogels were more conducive to cell proliferation than non-porous hydrogels because cells could migrate into the microporous pores and proliferate rapidly[26], whereas the high cell and ECM density of CSs

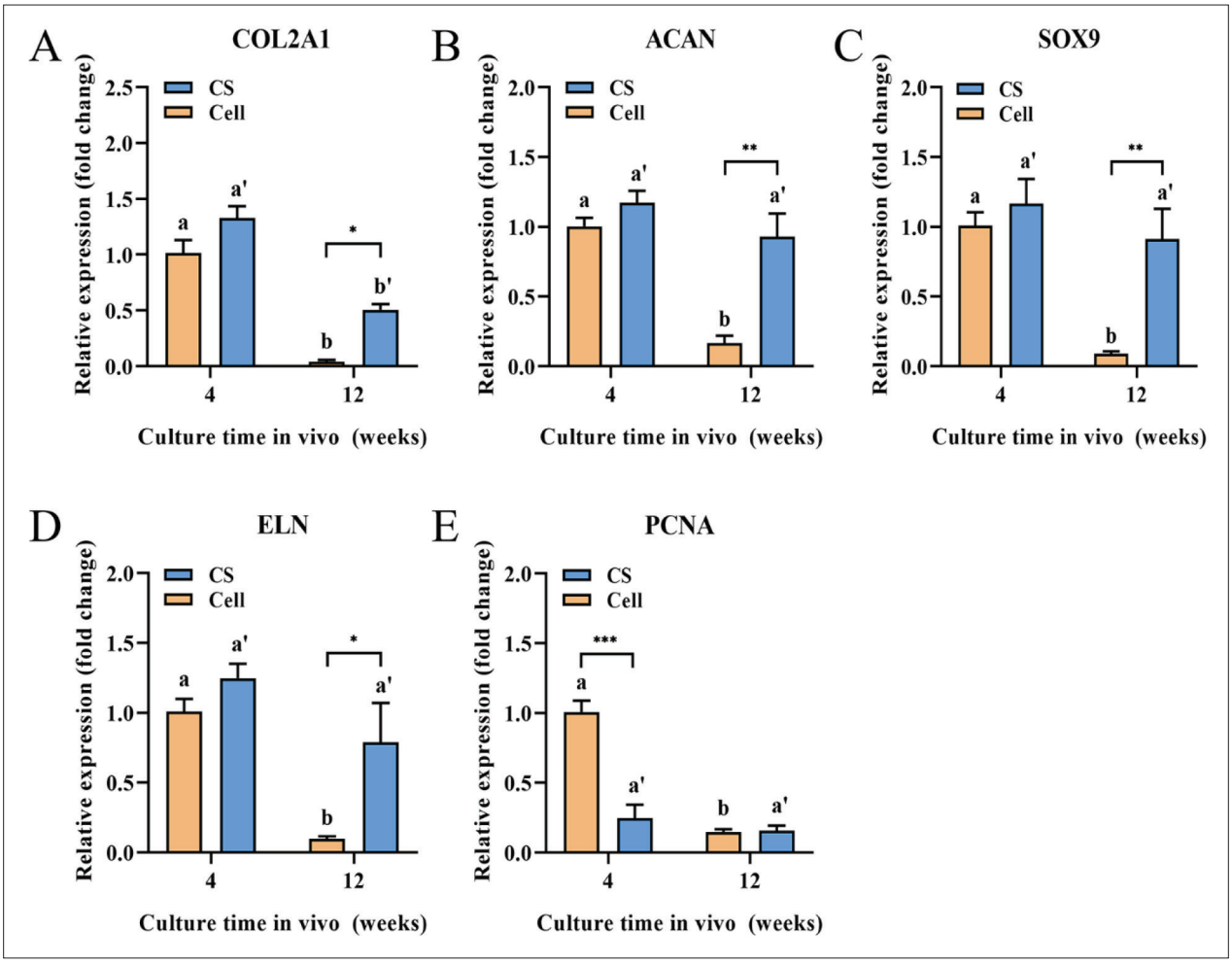

Figure 8. Gene expression analysis of printed constructs. Relative expression of (A) *COL2A1*, (B) *ACAN*, (C) *SOX9*, (D) *ELN*, and (E) *PCNA*. *$p < 0.05$; **$p < 0.01$; ***$p < 0.001$. Statistical analysis of the same group at different culture time is indicated by letters, and different letters represent $p < 0.05$. Statistical analysis between different groups is indicated by asterisks: *$p < 0.05$; **$p < 0.01$; ***$p < 0.001$.

made it more difficult for the cells therein to migrate into the micropores for proliferation compared to dispersed chondrocytes. On the other hand, when comparing the expression of these genes at different time points *in vivo*, the results showed that the expression levels of all these genes decreased to varying degrees in both groups. Notably, compared to the cell-laden group where all genes showed a significant decrease in expression levels at 12 weeks from 4 weeks, the CS-laden group showed only a significant decrease in *COL2A1*, which was still significantly higher than that of the cell-laden group. The possible explanation for the decreased expression of these genes is that in the early stage of implantation, the cells proliferate and secrete ECM actively, but with the prolongation of culture time and the secretion of ECM, the cells gradually become quiescent; however, since the adjacent cells and ECM in the 3D microenvironment of the CS-laden group can provide more dynamic and complex biological cues than the hydrogels[8], the cell function and phenotype are better maintained within the CS-laden group.

In summary, the use of CS-laden microporous bioinks for cartilage bioprinting allows better chondrocyte function and thus rapid regeneration of mature cartilage tissue, but the preparation method of CSs and the formulation of the hydrogels still need to be optimized to further promote cell proliferation, which is necessary for better cartilage regeneration.

4. Conclusion

In this study, we reported a functional bioink for cartilage bioprinting based on CSs and microporous hydrogels for the first time, with a focus on clarifying the influence of cell number and culture time on the CSs *per se* as well as the feasibility and effectiveness of the CS-laden microporous bioink in cartilage bioprinting. The results showed that

CSs with lower cell numbers and shorter culture time had better proliferation and growth potential in microporous hydrogels and were more suitable for cartilage bioprinting. In addition, our results demonstrated that the CS-laden bioink could be successfully printed into predefined lattice-shape constructs with little cell damage and regenerated cartilage tissue *in vivo* with a structure similar to natural cartilage characterized by typical lacunae structure and abundant cartilage-specific ECM deposition. Notably, the 3D microenvironment provided by the CSs enabled better function and phenotype of chondrocytes which was conducive to cartilage regeneration and maturation, but the rapid secretion of the ECM of CSs would limit the cell proliferation. Therefore, in the future, we will further adjust and optimize the CS-laden bioink to balance cell proliferation and function in order to achieve better cartilage regeneration.

Acknowledgments

None.

Funding

This work was supported by the Chinese Academy of Medical Sciences Innovation Fund for Medical Sciences (2021-I2M-1-052), the National Natural Science Foundation of China (81871575), and the Fundamental Research Funds for the Central Universities (3332022139).

Conflict of interest

The authors declare no conflict of interests.

Author contributions

Conceptualization: Ruiquan Liu, Xia Liu, Haiyue Jiang
Data curation: Ruiquan Liu, Litao Jia
Funding acquisition: Haiyue Jiang, Xia Liu
Investigation: Ruiquan Liu
Methodology: Ruiquan Liu, Litao Jia, Jianguo Chen, Yi Long, Jinshi Zeng, Siyu Liu
Formal analysis: Ruiquan Liu, Siyu Liu
Project administration: Haiyue Jiang, Xia Liu, Bo Pan
Supervision: Xia Liu, Haiyue Jiang
Writing – original draft: Ruiquan Liu
Writing – review & editing: Xia Liu, Haiyue Jiang

Ethics approval and consent to participate

Animal experiments were approved by the Animal Care and Experiment Committee of Plastic Surgery Hospital (201737).

Consent for publication

Not applicable.

Availability of data

The data used in this study are available from the corresponding author upon reasonable request.

References

1. Jessop ZM, Hague A, Dobbs TD, *et al.*, 2021, Facial cartilaginous reconstruction-A historical perspective, state-of-the-art, and future directions. *Front Surg,* 8: 680186.

http://doi.org/10.3389/fsurg.2021.680186

2. Cao Y, Sang S, An Y, *et al.*, 2022, Progress of 3D printing techniques for nasal cartilage regeneration. *Aesthetic Plast Surg,* 46(2): 947–964.

http://doi.org/10.1007/s00266-021-02472-4

3. Cao Y, Vacanti JP, Paige KT, *et al.*, 1997, Transplantation of chondrocytes utilizing a polymer-cell construct to produce tissue-engineered cartilage in the shape of a human ear. *Plast Reconstr Surg,* 100(2): 297–302; discussion 303–294.

http://doi.org/10.1097/00006534-199708000-00001

4. Tan B, Gan S, Wang X, *et al.*, 2021, Applications of 3D bioprinting in tissue engineering: Advantages, deficiencies, improvements, and future perspectives. *J Mater Chem B,* 9(27): 5385–5413.

http://doi.org/10.1039/d1tb00172h

5. Wang G, Zhang X, Bu X, *et al.*, 2022, The application of cartilage tissue engineering with cell-laden hydrogel in plastic surgery: A systematic review. *Tissue Eng Regen Med,* 19(1): 1–9.

http://doi.org/10.1007/s13770-021-00394-5

6. Tang P, Song P, Peng Z, *et al.*, 2021, Chondrocyte-laden GelMA hydrogel combined with 3D printed PLA scaffolds for auricle regeneration. *Mater Sci Eng C Mater Biol Appl,* 130(1): 112423.

http://doi.org/10.1016/j.msec.2021.112423

7. Zeng J, Jia L, Wang D, *et al.*, 2023, Bacterial nanocellulose-reinforced gelatin methacryloyl hydrogel enhances biomechanical property and glycosaminoglycan content of 3D-bioprinted cartilage. *Int J Bioprint,* 9(1): 631.

http://doi.org/10.18063/ijb.v9i1.631

8. Achilli TM, Meyer J, Morgan JR, 2012, Advances in the formation, use and understanding of multi-cellular spheroids. *Expert Opin Biol Ther,* 12(10): 1347–1360.

http://doi.org/10.1517/14712598.2012.707181

9. Kronemberger GS, Matsui RAM, Miranda G, *et al.*, 2020, Cartilage and bone tissue engineering using adipose stromal/stem cells spheroids as building blocks. *World J Stem Cells,* 12(2): 110–122.

http://doi.org/10.4252/wjsc.v12.i2.110

10. Zhang J, Xin W, Qin Y, *et al.*, 2022, "All-in-one" zwitterionic granular hydrogel bioink for stem cell spheroids production and 3D bioprinting. *Chem Eng J,* 430(50): 132713.

http://doi.org/10.1016/j.cej.2021.132713

11. Chen H, Tan XN, Hu S, *et al.*, 2021, Molecular mechanisms of chondrocyte proliferation and differentiation. *Front Cell Dev Biol,* 9: 664168.

http://doi.org/10.3389/fcell.2021.664168

12. Ghosh S, Laha M, Mondal S, *et al.*, 2009, In vitro model of mesenchymal condensation during chondrogenic development. *Biomaterials,* 30(33): 6530–6540.

http://doi.org/10.1016/j.biomaterials.2009.08.019

13. Chae S, Hong J, Hwangbo H, *et al.*, 2021, The utility of biomedical scaffolds laden with spheroids in various tissue engineering applications. *Theranostics,* 11(14): 6818–6832.

http://doi.org/10.7150/thno.58421

14. Decarli MC, Amaral R, Santos DPD, *et al.*, 2021, Cell spheroids as a versatile research platform: formation mechanisms, high throughput production, characterization and applications. *Biofabrication,* 13(3): 1-37.

http://doi.org/10.1088/1758-5090/abe6f2

15. Mironov V, Visconti RP, Kasyanov V, *et al.*, 2009, Organ printing: Tissue spheroids as building blocks. *Biomaterials,* 30(12): 2164–2174.

http://doi.org/10.1016/j.biomaterials.2008.12.084

16. Grevenstein D, Mamilos A, Schmitt VH, *et al.*, 2021, Excellent histological results in terms of articular cartilage regeneration after spheroid-based autologous chondrocyte implantation (ACI). *Knee Surg Sports Traumatol Arthrosc,* 29(2): 417–421.

http://doi.org/10.1007/s00167-020-05976-9

17. Gryadunova A, Kasamkattil J, Gay MHP, *et al.*, 2021, Nose to spine: Spheroids generated by human nasal chondrocytes for scaffold-free nucleus pulposus augmentation. *Acta Biomater,* 134(4): 240–251.

http://doi.org/10.1016/j.actbio.2021.07.064

18. Huang BJ, Hu JC, Athanasiou KA, 2016, Effects of passage number and post-expansion aggregate culture on tissue engineered, self-assembled neocartilage. *Acta Biomater,* 43(3): 150–159.

http://doi.org/10.1016/j.actbio.2016.07.044

19. Jeon JH, Yun BG, Lim MJ, *et al.*, 2020, Rapid cartilage regeneration of spheroids composed of human nasal septum-derived chondrocyte in rat osteochondral defect model. *Tissue Eng Regen Med,* 17(1): 81–90.

http://doi.org/10.1007/s13770-019-00231-w

20. Wang G, An Y, Zhang X, *et al.*, 2021, Chondrocyte spheroids laden in GelMA/HAMA hybrid hydrogel for tissue-engineered cartilage with enhanced proliferation, better phenotype maintenance, and natural morphological structure. *Gels,* 7(4): 247.

http://doi.org/10.3390/gels7040247

21. De Moor L, Minne M, Tytgat L, *et al.*, 2021, Tuning the phenotype of cartilage tissue mimics by varying spheroid maturation and methacrylamide-modified gelatin hydrogel characteristics. *Macromol Biosci,* 21(5): e2000401.

http://doi.org/10.1002/mabi.202000401

22. Kang HW, Lee SJ, Ko IK, *et al.*, 2016, A 3D bioprinting system to produce human-scale tissue constructs with structural integrity. *Nat Biotechnol,* 34(3): 312–319.

http://doi.org/10.1038/nbt.3413

23. Ying GL, Jiang N, Maharjan S, *et al.*, 2018, Aqueous two-phase emulsion bioink-enabled 3D bioprinting of porous hydrogels. *Adv Mater,* 30(50): e1805460.

http://doi.org/10.1002/adma.201805460

24. Ying G, Jiang N, Parra C, *et al.*, 2020, Bioprinted injectable hierarchically porous gelatin methacryloyl hydrogel constructs with shape-memory properties. *Adv Funct Mater,* 30(46).

http://doi.org/10.1002/adfm.202003740

25. Shi W, Shi H, Fu G, *et al.*, Application of agarose gelatin in tissue pre-embedding before dehydration. *J Clin Exp Pathol,* 37(3): 365–366.

http://doi.org/10.13315/j.cnki.cjcep.2021.03.031

26. Jia L, Hua Y, Zeng J, *et al.*, 2022, Bioprinting and regeneration of auricular cartilage using a bioactive bioink based on microporous photocrosslinkable acellular cartilage matrix. *Bioact Mater,* 16(1): 66–81.

http://doi.org/10.1016/j.bioactmat.2022.02.032

27. Van Winkle AP, Gates ID, Kallos MS, 2012, Mass transfer limitations in embryoid bodies during human embryonic stem cell differentiation. *Cells Tissues Organs,* 196(1): 34–47.

http://doi.org/10.1159/000330691

28. Lin RZ, Chang HY, 2008, Recent advances in three-dimensional multicellular spheroid culture for biomedical research. *Biotechnol J,* 3(9–10): 1172–1184.

http://doi.org/10.1002/biot.200700228

29. Shi W, Kwon J, Huang Y, *et al.*, 2018, Facile tumor spheroids formation in large quantity with controllable size and high uniformity. *Sci Rep,* 8(1): 6837.

http://doi.org/10.1038/s41598-018-25203-3

30. Niebruegge S, Bauwens CL, Peerani R, *et al.*, 2009, Generation of human embryonic stem cell-derived mesoderm and cardiac cells using size-specified aggregates in an oxygen-controlled bioreactor. *Biotechnol Bioeng,* 102(2): 493–507.

http://doi.org/10.1002/bit.22065

31. Sart S, Tsai AC, Li Y, *et al.*, 2014, Three-dimensional aggregates of mesenchymal stem cells: Cellular mechanisms, biological properties, and applications. *Tissue Eng Part B Rev,* 20(5): 365–380.

http://doi.org/10.1089/ten.TEB.2013.0537

32. Behan K, Dufour A, Garcia O, *et al.*, 2022, Methacrylated cartilage ECM-based hydrogels as injectables and bioinks for cartilage tissue engineering. *Biomolecules,* 12(2): 216.

http://doi.org/10.3390/biom12020216

33. Ozbolat IT, Hospodiuk M, 2016, Current advances and future perspectives in extrusion-based bioprinting. *Biomaterials,* 76: 321–343.

http://doi.org/10.1016/j.biomaterials.2015.10.076